Facilitating the design of combination therapy for cancer using multipartite network models: Emphasis on acute myeloid leukaemia

Mohieddin Jafari (mohieddin.jafari@helsinki.fi)
University of Helsinki https://orcid.org/0000-0002-6991-8587
Mehdi Mirzaie
Helsinki University
Jie Bao
Helsinki University
Farnaz Barneh
Princess Máxima Center
Shuyu Zheng
University of Helsinki https://orcid.org/0000-0003-0624-8077
Johanna Eriksson
Helsinki University
Jing Tang
Helsinki University

Article

Keywords: drug therapy, cancer treatments, myeloid leukaemia

Posted Date: June 22nd, 2021

DOI: https://doi.org/10.21203/rs.3.rs-577256/v1

Version of Record: A version of this preprint was published at Nature Communications on April 19th, 2022. See the published version at https://doi.org/10.1038/s41467-022-29793-5.

Facilitating the design of combination therapy for cancer using multipartite network models: Emphasis on acute myeloid leukaemia

Mohieddin Jafari[1*], Mehdi Mirzaie[1], Jie Bao[1], Farnaz Barneh[2], Shuyu Zheng[1], Johanna Eriksson[1], Jing Tang[1*]

[1]Research Program in Systems Oncology, Faculty of Medicine, University of Helsinki, Finland

[2]Prinses Maxima Center for Pediatric Oncology, 3584 CS Utrecht, the Netherlands

Corresponding authors:

Jing Tang

Tel. +358 45 8689708

Jing.tang@helsinki.fi

Mohieddin Jafari

Mohieddin.jafari@helsinki.fi

Abstract

From the drug discovery perspective, combination therapy is recommended for cancer treatment due to its efficiency and safety compared to the common cytotoxic and single-targeted monotherapies. However, identifying effective drug combinations is time-and cost-consuming. Here, we offer a novel strategy for predicting potential drug combinations and patient subclasses by constructing multipartite networks using drug-response data on patient samples. In this study, we used Beat AML and GDSC, two comprehensive datasets based on patient-derived and cell line-based samples, to show the potential of multipartite network modelling in combinatorial cancer therapy. We used the median values of cell viability to compare drug potency and reconstruct a weighted bipartite network that models the interaction of drugs and biological samples. Then, clusters of network communities were identified in two projected networks based on the topological structure of the networks. Chemical structures, drug-target networks, protein–protein interactions, and signalling networks were used to corroborate the intra-cluster homogeneity. We further leveraged the community structures within the drug-based multipartite networks to discover effective multi-targeted drug combinations and synergy levels, which were supported with more evidence using the DrugComb and ALMANAC databases. Furthermore, we confirmed the potency of selective combinations of drugs against monotherapy in *in vitro* experiments using three acute myeloid leukaemia (AML) cell lines. Taken together, this study presents an innovative data-driven strategy based on multipartite networks to suggest potential drug combinations to improve AML treatment.

Introduction

Studies on cases with advanced cancers have shown that less than 10% of patients have actionable mutations, and the improvement of outcomes is unobserved in a randomised trial of precision medicine based on genomic profiles (1). The current limitation of genomics-centric personalised medicine falls short of the enormous heterogeneity and lack of actionable and sustainable treatment options. With a few exceptions, patient genomic signatures with clinical pathology do not typically predict drug responses. More precisely, cancer can principally be considered a signalling disease, not a genetic disease. There is a wealth of data that has validated this hypothesis, including signalling behaviours involved in growth factor and nutrient responses, the process of entering and exiting the cell cycle, ensuring that chromosomes are segregated in an orderly, efficient and accurate manner during mitosis and apoptosis (2, 3). On the other hand, the complexity of crosstalk between signalling pathways necessitates to modify multiple targets in cancer cells; otherwise, a lack of complete response, resistance, and relapse will emerge during the course of treatment.

Despite the fact that large amounts of small molecules or drugs have been tested on many cell lines or patient-derived samples, using single drugs as monotherapies to cure cancer might not be a promising strategy, as it is known that the complex interactions of various biological components can induce drug resistance during the treatment of cancer (4-6). As a matter of fact, monotherapy, the slogan of *one target one drug*—is inefficient in curing complex diseases, such as cancer (7, 8). Combination therapy or polytherapy with synergistic drugs may achieve a more effective and safer outcome by targeting several targets in the same or separate pathways of the complex system (4). To better identify the synergistic drug combination based on precision medicine, we need *ex vivo* drug screening to decipher the functional impact of cancer genomics at the phenotypic level and to understand their interactions in the context of biological networks (9, 10). Therefore, understanding network biology may provide a unique opportunity to leverage the rich source of drug response data to offer network-based models for combinatorial therapy. These network models have shown promise for developing clinical decision support tools to discriminate functional patient subclasses (11, 12). Even though there are networks reconstructed to model biological mechanisms of diseases and predict drug combination synergies based on molecular data (13-16), network models have not been systematically applied to patient data, such as the drug response data of patient-derived samples, to predict patient-customised drug combinations (14). Instead, the *ex vivo* drug response data are straightforwardly translated into the clinic for patient treatment since these individualised

experiments represent the efficiency of some approved drugs on patient-derived primary cultures (17, 18).

In 2018, the Beat AML programme reported a cohort of 672 tumour specimens collected from 531 patients, analysing the *ex vivo* sensitivity for 122 drugs alongside the mutational status and the gene expression signatures of the samples (19). Despite the dearth of large patient-related drug response datasets, some large cell line–based datasets, such as genomics of drug sensitivity in cancer (GDSC) and ALMANAC, can offer a strong source of supporting evidence for predictions. The GDSC database contains the responses of 1001 cancer cell lines to 265 anti-cancer drugs, providing a rich source of information to connect genotypes with cellular phenotypes and to identify cancer-specific therapeutic options (20). The largest publicly accessible dataset for cancer combination drugs, such as ALMANAC, was recently published by the U.S. National Cancer Institute. This data collection contained more than 5,000 combinations of 104 investigational and licensed drugs, with synergies calculated against 60 cancer cell lines, resulting in more than 290,000 synergy scores (21). Moreover, DrugComb (https://drugcomb.org/), a web-based portal for storing and studying drug combination screening datasets, offers a comprehensive visualisation of drug combination susceptibility and synergy, which can significantly aid in the understanding of drug interactions at unique dosage levels. Drugcomb now has 751,498 drug combinations and 717,684 single drug screens from 37 trials, which relate to 2040 cell lines and 216 cancer forms (22).

In this study, we developed a network pharmacology approach to predict potential drug combinations for acute myeloid leukaemia (AML) based on the Beat AML dataset. We proposed a drug combination strategy using multipartite network modelling of *ex vivo* drug screening data. By *ex vivo* drug response data, we directly accessed the individual phenotypes of the patients' cancer cells, and by network modelling, we demonstrated the similarity of drugs and AML patients. Then, we used the community structures within the drug-based multipartite networks to discover effective multi-targeted drug combination regimens. Our predicted drug combinations were only suggested regarding the phenotypic interactions of the cancer cells or patient samples with the drugs without prior understanding of the genetic origin or molecular understanding of the disease.

Methods

Fig. 1 presents the entire workflow of this study. The weighted bipartite network is constructed using the Beat AML dataset. This dataset is a collaborative research programme of 11 academic medical centres providing data on AML samples while offering genomics, clinical, and drug responses. It includes a cohort study of 672 tumour specimens collected from 531 patients and an analysis of 122 drug responses. To construct a weighted bipartite network, the best response read-out of drug potency was defined using information-based measures. Then, two unipartite networks were obtained using network projection on the samples and drugs. Next, communities of two projected networks were extracted, and intra-cluster homogeneity analysis was performed using the similarity of drugs and patients/cell members based on available gene expression profiles for patients, protein–protein interaction network, and biological pathways. The drug candidates for drug combination were selected from two different communities, and a high-throughput drug screening was used to assess their synergetic effects.

Defining the response read-out for drug screening experiments

Pharmacogenomic studies require extensive standardisation to avoid inconsistency of drug response data for further research and unbiased predictions (23, 24). Therefore, first, we controlled the quality of cell viability data to select the potent compounds. To achieve this, we examined the raw datasets regarding the availability of replicated data and outlier detection, followed by assessment of distribution, pairwise correlation, and homoscedasticity analyses to select the best response read-out or measure of drug potency. This analysis was performed using information-based nonparametric measures available in the Minerva package (25) by computing the maximal information coefficient (MIC), maximum edge value (MEV), and maximum asymmetry score (MAS). Furthermore, the relative and absolute IC50 (i.e. IC50 measures, which were computed based on the top and bottom plateaus of the curve or based on the blank and the positive control values, respectively), relative inhibition (RI) value, area under curve of drug-response fitted line (AUC), and the median of cell viability in the drug response experiments were

assessed to select the best measurement. The chosen measurement was later used as a weight value for the edges of the weighted bipartite network reconstruction.

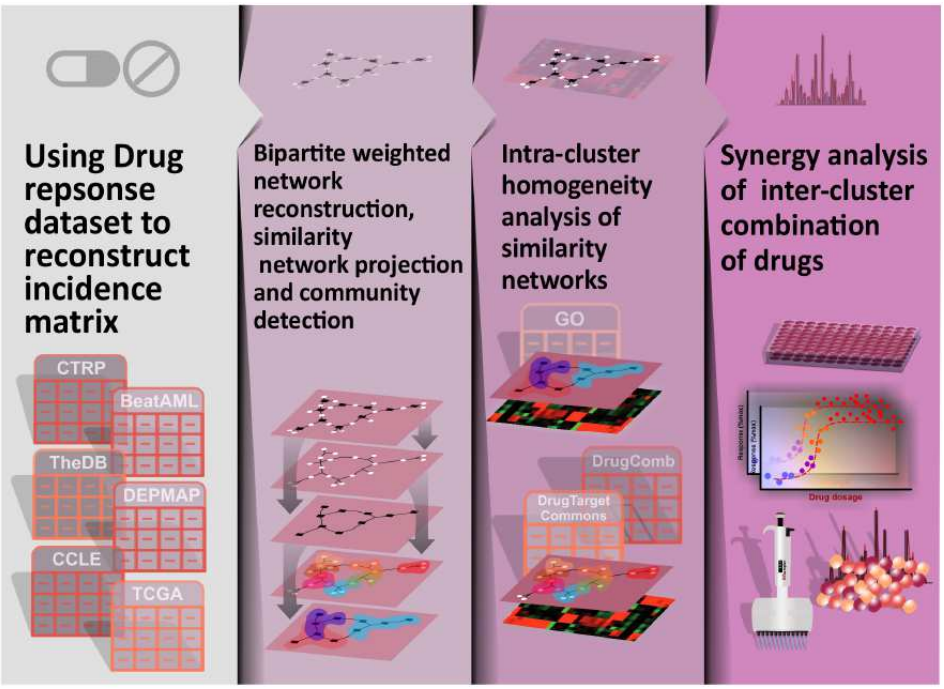

Figure 1: Flowchart of the study

Data collection started from existing drug response databases, followed by incidence matrix extraction, weighted bipartite network reconstruction, network projection, and community detection. Furthermore, the intra-cluster homogeneity analysis was conducted using the similarity of drug and patient/cell members of all clusters according to available gene expression profiles, drug–target interactions, protein–protein interactions, and biological pathways. Finally, a high-throughput drug screening experiment was used to assess the synergistic behaviour of the proposed drug combinations.

Reconstruction and analysis of the bipartite network model

In our bipartite network model, one group of nodes contained drugs and the other group contained cancer cell lines (in GDSC and ALMANAC) or patient samples (in BeatAML). The edges were defined by incidence matrices derived from the min–max normalised values:

$$Normalised\ value = \frac{\text{value} - \text{minimum}(values)}{\text{maximum}(values) - \text{minimum}(values)}.$$

This normalisation transforms these values, which indicate the potency of small molecules on cancer cell lines or patient samples, into a decimal between 0 and 1. Next, we projected the bipartite network into two similarity networks: the drug similarity network and sample similarity network. In the network projection, two unipartite graphs were derived from a bipartite graph, resulting in the deduction of a similar node's relationships. In this study, we projected similarity networks that consider the edge weights in the bipartite network. Then, we studied the general properties of the networks, such as network heterogeneity, centralisation,

and clustering coefficients. The critical step was community detection within the projected networks to discern functionally similar drugs and cells or patients regarding drug response. The modularity index was used to determine the best community detection algorithms, including infomap (26), fast greedy (27), and spinglass (28). Furthermore, we explored the network modules to propose a strategy for drug combination design.

Computational corroboration

Multiple computational methods were applied to validate the predictions of the drug combinations and patient or cell stratification. The validation of the community structures is like the general cluster quality assessment method, and we assessed the clustering performance by matching the clustering structures to prior knowledge. This validation is foundational to possible drug combination designs. Alternatively, the combination of distinct drugs in terms of chemical structure, target profile, and implicated biological pathways is likeliest more efficient than similar drugs (7). Therefore, we used the drug–target network, protein–protein interactions, and signalling networks to justify the similarity of cluster elements. Thus, Chembl (29), drug target commons (DTC) (30), KEGG (31), and the OmniPath database (32) were used to extract prior annotations about the drugs and their targets. To compare the chemical structures of the drugs, a simplified molecular input line entry system (SMILES) of the drug molecules was retrieved and transformed into an extended connectivity fingerprint (ECFP) to assess the Dice similarity of the molecules. The Dice similarity is one of the standard metrics for molecular similarity calculations in which $S_{A,B} = {}^{2c}/_{(a+b)}$, where a is the number of ON bits in molecule A, b is the number of ON bits in molecule B, and c is the number of ON bits in both A and B molecules (33). Also, the corresponding gene expression profiles were used to assess similarity within a patient or cell line modules in the sample similarity networks. For reads per kilobase per million (RPKM) with negative values and counts per million (CPM), we used the Harmonic similarity and Jaccard distance, respectively, as follows:

$S_{P,Q} = 2 \times \sum_{i=1}^{n} (P_i \times Q_i)/(P_i + Q_i)$,

$D_{P,Q} = 1 - \sum_{i=1}^{n} (P_i \times Q_i)/\left(\sum_{i=1}^{n} {P_i}^2 + \sum_{i=1}^{n} {Q_i}^2 + \sum_{i=1}^{n} P_i \times Q_i\right)$, where $P = \{P_1, P_2, \cdots, P_n\}$ and $Q = \{Q_1, Q_2, \cdots, Q_n\}$ denote the vector of gene expression values for patients or cell lines, and n is the number of genes. In all cases, the similarity or distance scores were compared with the random grouping of small molecules or biological samples to perform statistical testing.

The synergy scores provided by the DrugComb database (34) were used to corroborate synergistic combinations of our network-based predictions, including HSA, Bliss, Loewe, ZIP, CSS, and S. Let us assume that drug 1 at dose x_1 and drug 2 at dose x_2 are used to produce the effects of y_1 and y_2 , and y_c is the effect of their combination. Drug effect is usually measured as a percentage of cell death, and a drug combination is classified as synergetic, antagonistic, or non-interactive (35). The expected effect denoted by y_e represents a non-interactive level, and it is quantified based on a reference model. Several mathematical models have been introduced to calculate the expected effect by assuming specific principles. The HSA model (36) considers the expected combination effect as the maximum of single-drug effects, that is, $y_e = \max(y_1,y_2)$. The Loewe model (37) assumes that an individual drug produces y_e at a higher dose than in the combination. In the Bliss model (38), y_e is the effect of the two drugs acting independently. The ZIP model (35) considers the assumptions of the Loewe and Bliss models by assuming that, at the reference model, two drugs do not potentiate each other. CSS determines the sensitivity of a drug pair, and S synergy is based on the difference between the drug combination and the single drug dose–response curves (39).

Cell culture and reagents

AML cell lines MOLM-16, NOMO-1, and OCI-AML3 were kind gifts from Professor Caroline Heckman (University of Helsinki, Finland). MOLM-16 and NOMO-1 were cultured in RPMI-1640 medium (Gibco/Thermo Fisher Scientific, Waltham, MA, USA) and OCI-AML3 in α-MEM (with nucleosides; Gibco/Thermo Fisher Scientific) supplemented with GlutaMAX (Gibco CTS/Thermo Fisher Scientific), foetal bovine serum (20% for MOLM-16 and OCI-AML3; 10% for NOMO-1), and antibiotics.

Drug combination testing

The compounds dissolved in dimethyl sulfoxide (DMSO) were plated using Beckman Coulter Echo 550 Liquid Handler (Beckman Coulter, Indianapolis, IN, USA) combined with seven concentrations for each compound in half-log dilution series with 2.5/7.5/25 nl volumes, covering a 1,000-fold concentration range on black clear-bottom TC-treated 384-well plates (Corning #3764, Corning, NY, USA). All doses were randomised across the plate to minimise any plate effects. As positive (total killing) and negative (non-effective) controls, 100 μM of benzethonium chloride and 0.2% DMSO were used, respectively.

Cells were plated on pre-administered compound plates in 25 μl (2500, 2000, or 1250 cells per well for MOLM-16, NOMO-1, and OCI-AML3 cell lines, respectively) using BioTek MultiFlo FX RAD (5 μl cassette) (Biotek, Winooski, VT, USA) and incubated for 72 h at 37°C and 5% CO2. Cell

viability was then determined by dispensing 25 µl of Cell Titre Glow 2.0 reagent (Promega, Madison, WI, USA). Plates were incubated for 5 min and centrifuged for 5 min (173 × g) before reading luminescence with a PHERAstar FS multimode plate reader (BMG Labtech, Ortenberg, Germany).

Results

Defining the edge weight of bipartite networks

In the Beat AML dataset, a set of 122 inhibitor drugs was used against 531 patient-derived AML samples. The spectra of low to high potency of drugs were observed across the patient-derived samples. However, this panel of small molecule inhibitors was selected according to their activity against the proteins involved in tyrosine-dependent and non-tyrosine kinase pathways, particularly for AML (19). First, we determined the weight value of the drug–sample interaction to be used in the bipartite network reconstruction. This value should describe the most potent compounds for inhibiting tumour cells regarding the drug sensitivity analysis. Adding to the relative and absolute $IC_{50,}$ RI value (39), and AUC, we calculated the median cell viability in the drug response experiments. The distribution of these measures was evaluated in terms of normality, skewness, and modality (Fig. 2) to choose the best measure as a weight in the bipartite network. The relationship of median to AUC was a high positive value (with the highest r Pearson correlation coefficient ~ 0.94). The distribution of medians was unimodal in contrast to IC_{50} distributions, homoscedastic contrary to RI distribution, and more symmetric (non-skewed) compared to AUC distribution. In addition to investigating the linear relationship, that is, Pearson correlation analysis, we computed MIC, which measures the relationship strength, and MEV to check the closeness of the relationship to being a function. Interestingly, the relationship between median and AUC displayed higher MAS and MEV (~0.75) compared with the relationship of RI and AUC, meaning that median has a stronger association with AUC. Therefore, we have chosen the inverse of the actual median as the weight of the drug–patient interaction.

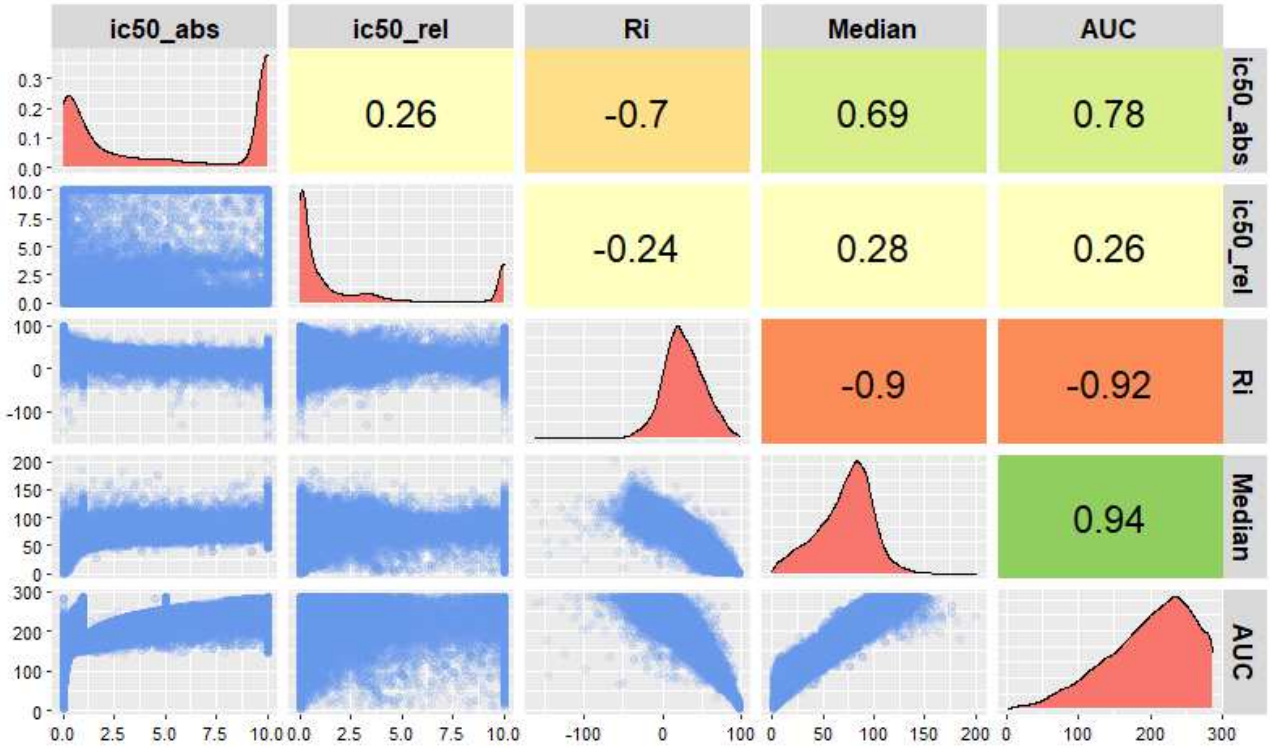

Figure 2: Comparison of different measures for drug response experiments in the Beat AML study. The lower triangle of this pairwise comparison matrix shows the pairwise scatter plots for ic50_abs (Absolute IC_{50}), ic50_rel (Relative IC_{50}), RI (Relative Inhibition), median (the median of cell viability), and AUC (Area Under Curve of cell viability fitted line). The diagonal panel describes the histogram of each measure independently. The upper triangle represents the Pearson correlation coefficients of the corresponding pairwise comparisons.

Analysis of bipartite networks

Furthermore, the maximum square submatrix of patient samples and small molecules was used as the incidence matrix of the bipartite network. Specifically, we selected the list-wise deletion strategy to remove missing values, and we used the complete cases of both variables. The downstream analysis was done on an undirected weighted bigraph comprising 176 (88 + 88) nodes and 7744 edges (Fig. 3A). The distribution of the min–max normalised edge weights indicated positive skewness, indicating that the cells were not highly sensitive to most drugs. All the performed analyses were also carried out for the GDSC dataset as proof of concept. The undirected weighted bigraph of the GDSC dataset comprised 532 (266 + 266) nodes and 70,756 edges (Fig. 3C). The distribution of the min–max normalised edge weights showed positive skewness in this dataset as well (Fig 3D), again indicating low potency for most of the drugs. Therefore, exploring the best combination is not straightforward, and categorising drug–sample

interactions seems to be required. Following the projection of these bigraphs as outlined in Fig. 3, two projected graphs, the patient similarity network (PSN) and drug similarity network (DSN), were reconstructed, such that each edge was obtained by multiplying the weighted incidence matrix. Thus, the edge weights of the projected graphs indicate the profile similarities of patient samples in PSN and small molecule inhibitors in DSN. Note that the edge weight values in DSNs and PSNs differ due to the different matrix multiplications.

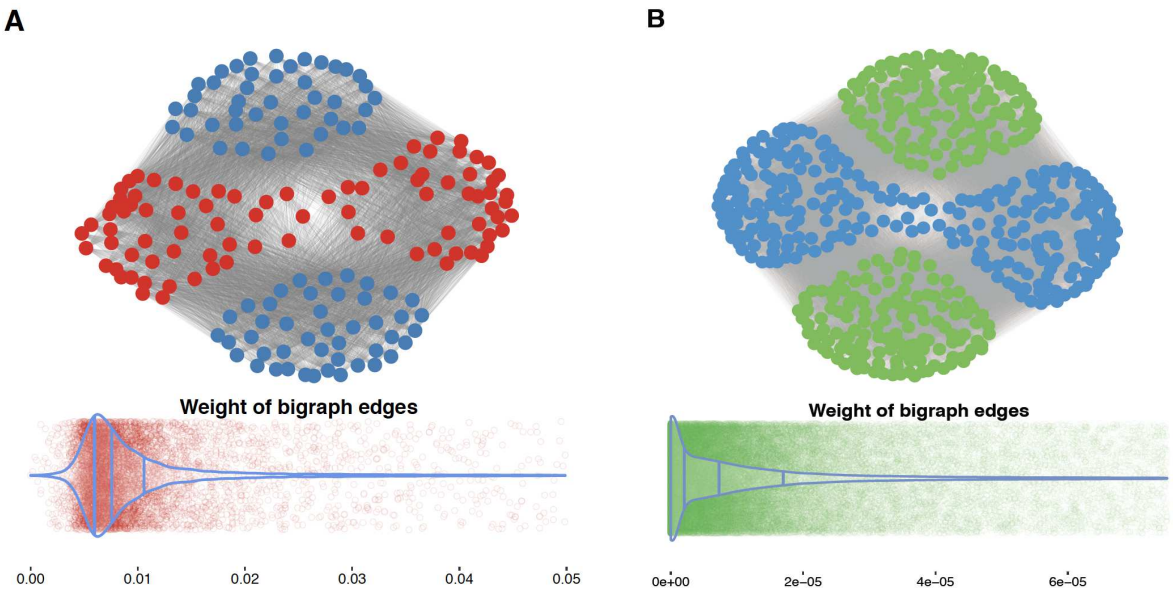

Figure 3: Bigraphs of cancer datasets. The general overview of the bipartite graphs for the Beat AML (A) and GDSC (B) datasets is represented with the blue nodes as small molecule inhibitors, and red and green nodes as patient-derived and cell line samples, respectively. The distributions of edge weight values are also depicted using violin plots with scatter plots.

The PSN and DSN of the Beat AML dataset contained 88 nodes and 3828 edges (Fig. 4), while in the GDSC projected similarity networks, there were 266 nodes and 35,378 edges (data not shown). In Fig. 4, the larger the node size, the more sensitive patient-derived samples and the more potent drugs. In this subset of the Beat AML dataset, without missing data, patient 16–00627 was found to be the most sensitive and SNS-032 was the most potent inhibitor (See Supplementary Fig. 1). The community detection was subsequently done for both similarity networks via modularity score optimisation, resulting in two communities for DSN with 50 and 38 small molecules, and two communities for PSN with 39 and 49 patient samples. Alternatively, we identified two clusters of patients with distinctive drug response profiles, suggesting two subcategories of the disease. Also, we detected two clusters of small molecules, which pointed to

disparate inhibiting patterns on the patient samples. In the following steps, we presented evidence of the consistency of cluster members in both networks using prior knowledge.

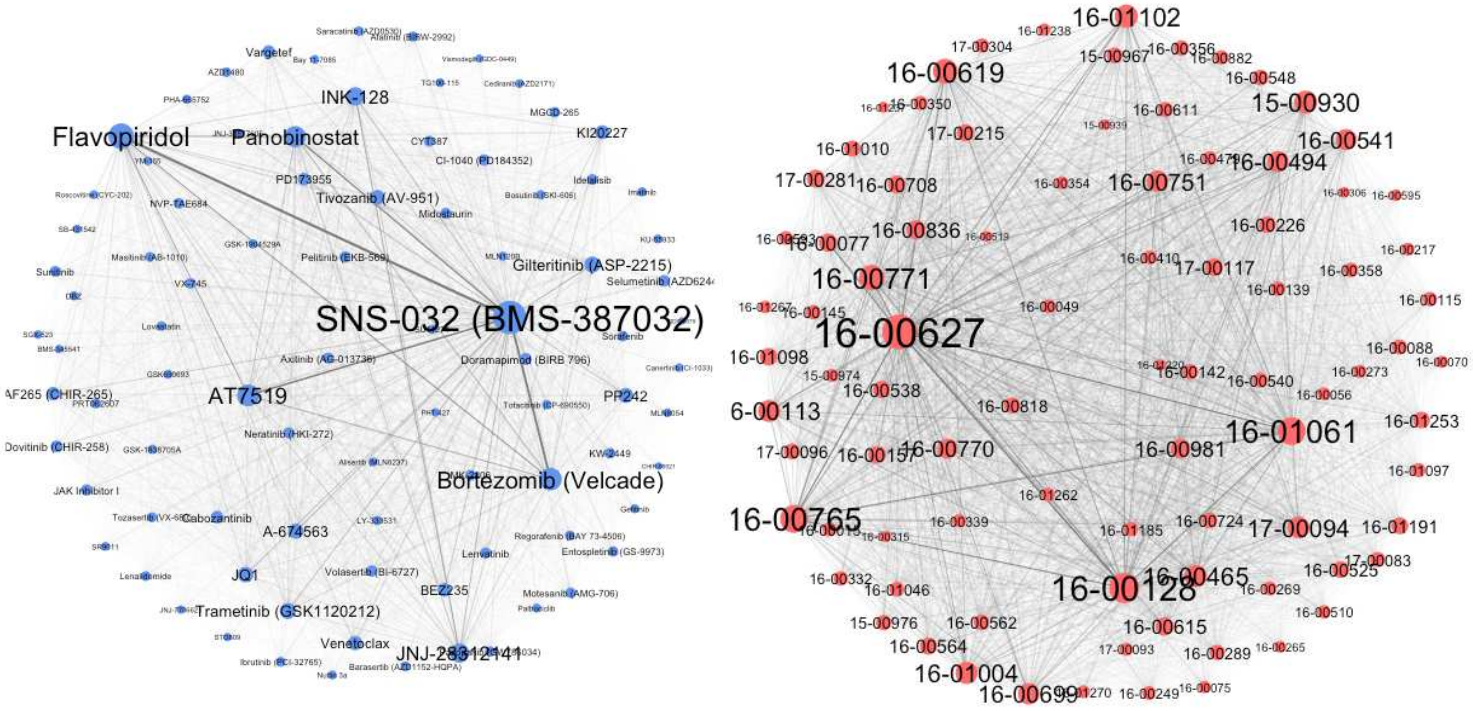

Figure 4: Drug and PSNs of the Beat AML dataset. The force-directed layout was selected to depict both networks. The thickness of the edges corresponds to the edge weight of the original bipartite networks after network projection, considering the weight values. The edge thickness represents the weight value of similarity between each pair of patient samples or small molecules. The node size is proportional to the strength of each node, which is the sum of the edge weights of the adjacent edges for each node.

Intra-cluster homogeneity analysis of similarity networks

Drug similarity network

Focusing on small molecules, we presumed that inhibitory molecules with correlated effects on cell survival tended to have similar structures, purposes, and functions (40-43). Therefore, we evaluated the similarity of SMILES structures, the analogy of protein targets, and the biological pathways of the detected clusters in the DSNs against random groupings of molecules. The distribution of the Dice similarity of the SMILES structures differed significantly between the random grouping and the clusters based on network topology (Fig. 5A). The statistical test of the median difference also resulted in the lowest p-values for both the pairwise two-sample Wilcoxon and Kruskal–Wallis rank sum test (p-value < 2e−16). Evaluating their target similarities, we explored the protein targets of the small molecule inhibitors and examined the number of target intersections of small molecule pairs within the clusters. In this analysis, DTC

and OmniPath were applied to explore the binding targets of small molecules and second-order node neighbours (secondary targets) in the signalling network, respectively. Assuming that proteins usually correspond to multiple signalling pathways, the KEGG database was used to check the number of pathway intersections of the protein targets for each pair of small molecules. The median similarity measures of the intersections within the network clusters significantly exceeded those for a large set of random pairs of small molecules (Fig. 5B–D) (p-value < 2.2e−16, Kruskal–Wallis rank sum test). Analysis of the GDSC dataset gave similar results (Fig. 6) (p-value < 2.2e−16, Kruskal–Wallis rank sum test), suggesting that our method is also reproducible for the analysis of cell line-based datasets.

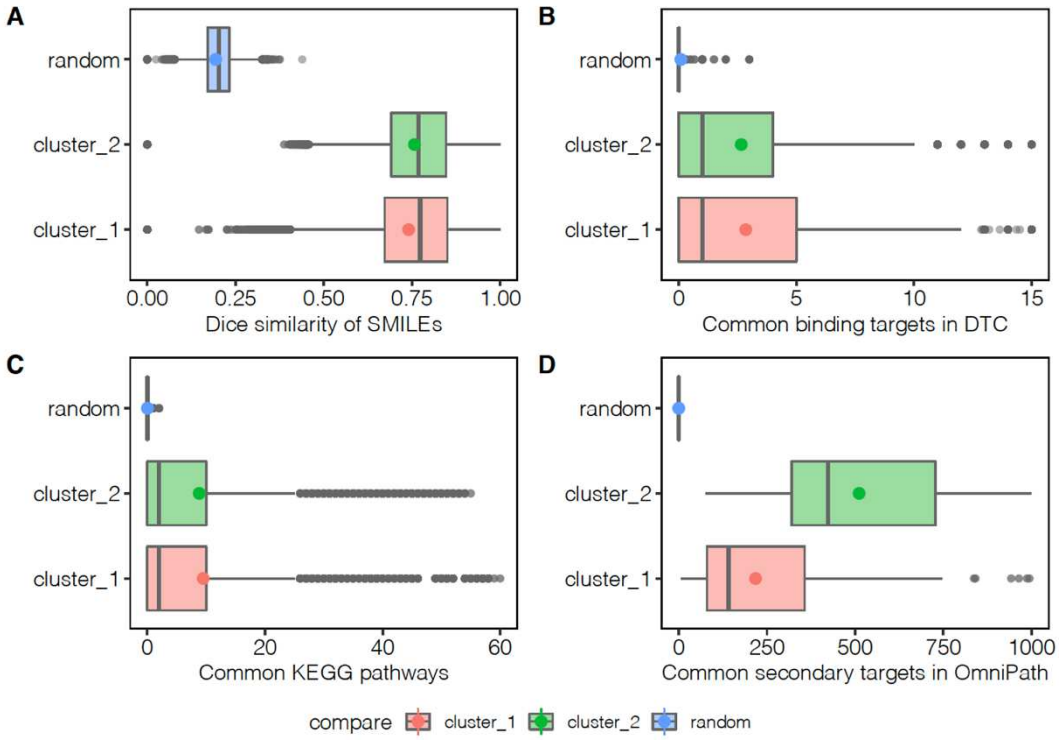

Figure 5: Beat AML intra-cluster homogeneity analysis. (A) The distribution of SMILE structure similarities of DSN clusters compared to random grouping. (B) The distribution of pairwise intersection size of binding protein targets, (C) corresponding KEGG pathways, and (D) secondary targets in the OmniPath database.

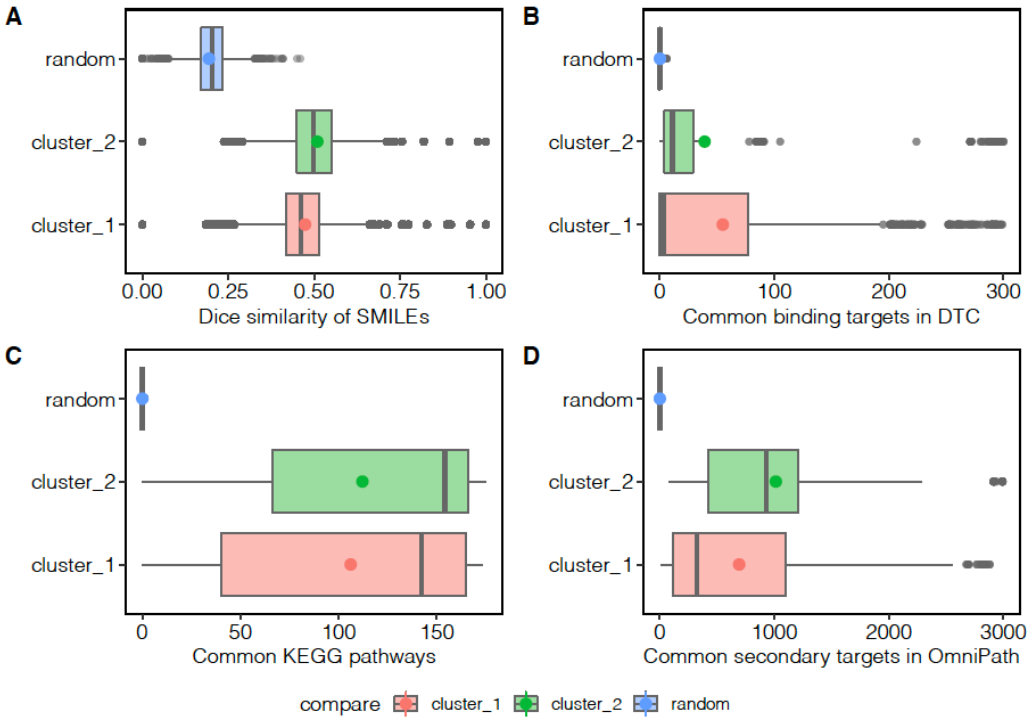

Figure 6: GDSC intra-cluster homogeneity analysis. (A) The distribution of SMILE structure similarities of DSN clusters compared to random grouping. (B) The distribution of pairwise intersection size of immediate protein targets, (C) corresponding KEGG pathways, and (D) second targets in the OmniPath database.

Patient and cell-line similarity network

Next, we examined the member consistency of the patient clusters in the PSN using other available data from patient samples in the Beat AML dataset. The gene expression data, including the RPKM and CPM of the samples, were utilised to check the pairwise similarity of the cluster members. The similarity measures were also computed for a large set of random pairs of patient samples to compare with our patient stratification using network clustering. When we compared the harmonic mean similarities of the RPKM values, the pairwise similarities of patients within the clusters significantly exceeded those of the randomly selected patients (p-value < 2.2e−16, Kruskal–Wallis rank sum test) (Fig. 7A). For the CPM dataset, the distributions of Jaccard distance were shown, where the distances within the clusters were statistically lower than those in the random group (p-value = 4.655e−05, Kruskal–Wallis rank sum test) (Fig. 7B). For the GDSC dataset, we used the expression profiles of signature genes provided by the SPEED platform (44). Then, differentially expressed genes were used to provide gene signatures of perturbed cancer-related pathways. In this dataset, there were 11 activity scores to represent the activity levels of 11 well-known pathways for each cell line. Therefore, we compared the distance distributions of the cell line pairs in the clusters to a set of random pairs of cell lines. Our findings indicated that

the distances within the clusters were much lower than those in the random grouping (p-value = 6.94e−08, Kruskal–Wallis rank sum test) (Fig. 7C).

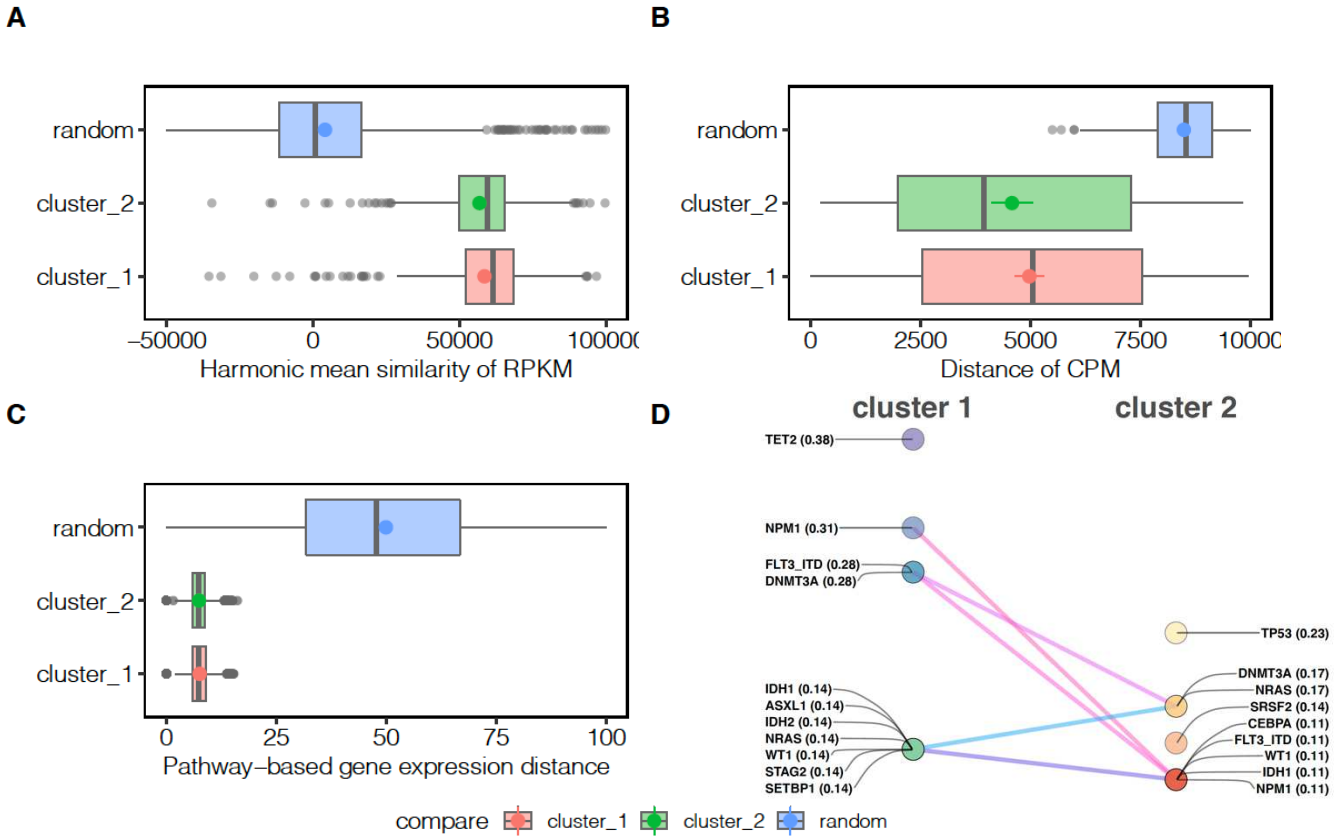

Figure 7: Validation of network communities of PSN. (A) The distribution of similarity of RPKM in the Beat AML dataset. (B) The distribution of distances of CPM in the Beat AML dataset. (C) The distribution of distances of pathway-based activity scores in GDSC dataset. (D) The frequently mutated genes in the clusters of Beat AML patients. The non-benign mutations with the possibility of being damaged in greater than 0.5 were selected to find the intersection of mutated genes. The gene names are shown with the relative frequency of mutated genes in each cluster (e.g. NPM1—0.38 indicates 38% of the patients in cluster 1 have this mutation). The lines between mutated genes illustrate the rank shift in the two clusters.

The Beat AML study also provided the first detailed view of the mutational landscape in AML. Here, we used a dataset of non-benign gene mutations to characterise both clusters of patient samples. As shown in Fig. 7D, both clusters of patients demonstrate a distinct profile of gene mutations regarding the involved genes and the ranks of genes based on frequency. Previously, Tyner et al. highlighted the importance of *TP53* and *ASXL* gene mutations, both responsible for the broad drug resistance patterns (19). They further showed that mutations in certain genes may identify disease subgroups sensitive to certain inhibitors. For example, they found that patients with FLT3-ITD and *NPM1* mutations were sensitive to SYK inhibitors.

Interestingly, our molecular-independent network-based approach to characterise patient samples also captured the significance of the mutations above. Furthermore, our findings indicate that *TP53*, *DNMT3A*, and *NRAS* were the most frequently mutated genes in one of the patient clusters, while *TET2* and *NPM1* were the most frequently mutated genes in the other cluster, along with the FLT3-ITD mutation. These results suggest that the phenotype-level information in drug response data can corroborate the genotype-level information to stratify patients more effectively.

Inter-cluster design strategy for drug combinations

We assumed that the best drug combination strategy was the selection of one drug from each cluster to block potential drug resistance mechanisms and cancer recurrence. A common drug combination design could be the use of the most effective drugs of each cluster to prohibit cancer cells more effectively. However, other pharmacologic evidence can encourage the choice of the best combination of drugs more specifically. As the focus in drug combination studies also lies in finding the most synergistic drug combinations, previously reported studies were used to explore the synergy values (i.e. the degree of interactions) of drug combinations. First, we checked if the combinations of the top five drugs (based on the median values of cell viability) of each cluster in the Beat AML and GDSC datasets (Table 1) were found in the DrugComb database. However, there were no reports regarding the 25 possible combinations of these drugs, so we aimed to compare the average synergistic values for these 10 drugs in the whole database. Fig. 8 shows the distributions of synergy values in DrugComb, highlighting the mean of the synergy of the bottom and top five drugs in each network cluster. This analysis revealed the reasonably high potential of the combinations of the top five drugs according to the average median values in both Beat AML and GDSC datasets (p-value = 2.96e−02 and p-value = 3.56e−02, Wilcox rank sum test, respectively).

Table 1: Top five small molecules in each cluster of DSNs

	Cluster 1	Cluster 2
Beat AML	SNS-032 (BMS-387032)	Dovitinib (CHIR-258)
	Flavopiridol	Nintedanib
	Panobinostat	Doramapimod (BIRB 796)
	AT7519	KI20227
	Bortezomib (Velcade)	Cabozantinib
GDSC	Amuvatinib	Sepantronium bromide (YM-155)
	GSK690693	Belinostat

	Vinblastine	AT-7519
	AS605240	CAY10603
	HG6-64-1	AR-42

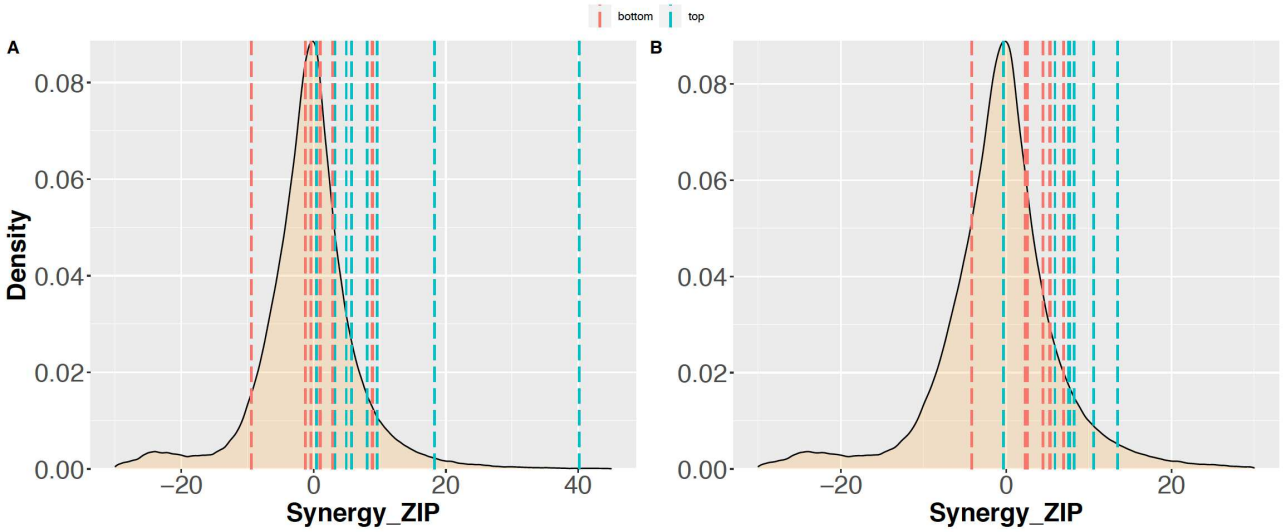

Figure 8: Distribution of drug combination synergy scores in the DrugComb database. The median of synergy zip score for the top and bottom five drugs are represented by dashed lines in Beat AML dataset (A) and the GDSC dataset (B).

Synergy analysis of the inter-cluster combination of drugs

For further validation of our strategy for predicting synergistic drug combinations using network modelling, we focused on the ALMANAC dataset (21), which has 1,892,650 combinations of 103 inhibitors tested on 60 cell lines. The same procedure as described in Fig. 1 was implemented to extract the drug modules in the DSN according to the available single drug experiments in this dataset. The median inhibition values of the single-drug responses on cell lines were used as weight values in the bipartite drug-cell line network. Using the projection of the weighted DSN, clusters of drugs with similar effect profiles on cell lines were extracted.

According to our predefined assumption, the combinations of drugs from different clusters were used as the positive group and the combinations of drugs within the clusters as the negative group. Then, we retrieved the synergy and sensitivity scores of the combinations for both groups using the DrugComb computed values, especially the highest single agent (HSA), zero-interaction potency (ZIP), Bliss, Loewe, combinational sensitivity score (CSS), and S synergy. Fig. 9A shows that the positive group of drug combinations exhibited a significantly higher value of drug synergy than the negative group. This result was evident for all types of synergy measures, indicating the superiority of the strategy of using inter-cluster drug combinations. These data

also indicate the efficiency of our proposed network-based modelling to discern drugs with similar profile effects on biological samples. Also, our proposed strategy of drug combination using the drugs of contrary clusters is likelier to acquire higher drug synergy and potency.

High-throughput drug screening for the proposed drug combinations in AML cell lines

To further demonstrate the ability of our model in predicting specific and robust drug combinations, experimental corroboration was conducted on a subset of 45 drug combinations for 3 AML cell lines, MOLM-16, OCI-AML3, and NOMO-1. Also, 25 out of 45 drug combinations originated from the top five drugs of the two clusters as the positive group, where higher synergy was predicted by our model, while others were the combinations of the top five drugs within each cluster, which transformed into 20 combinations as the negative group. The findings of the experimental validation of 135 drug-drug-cell line triplets is depicted in Fig. 9B using the ZIP, Bliss, HSA, and Loewe models to assess the degree of synergy. The drug combinations predicted by our model in the positive group were validated as more synergistic when considering positive scores as evidence of synergy degree (Fig. 10 and Supplementary Fig. 2). These findings were statistically more significant when using Bliss or HSA measures. Overall, these results demonstrate the robustness of network-based predictions across various experimental setups and synergy scoring models, and the ability of our network-based model to detect new combinations of treatments.

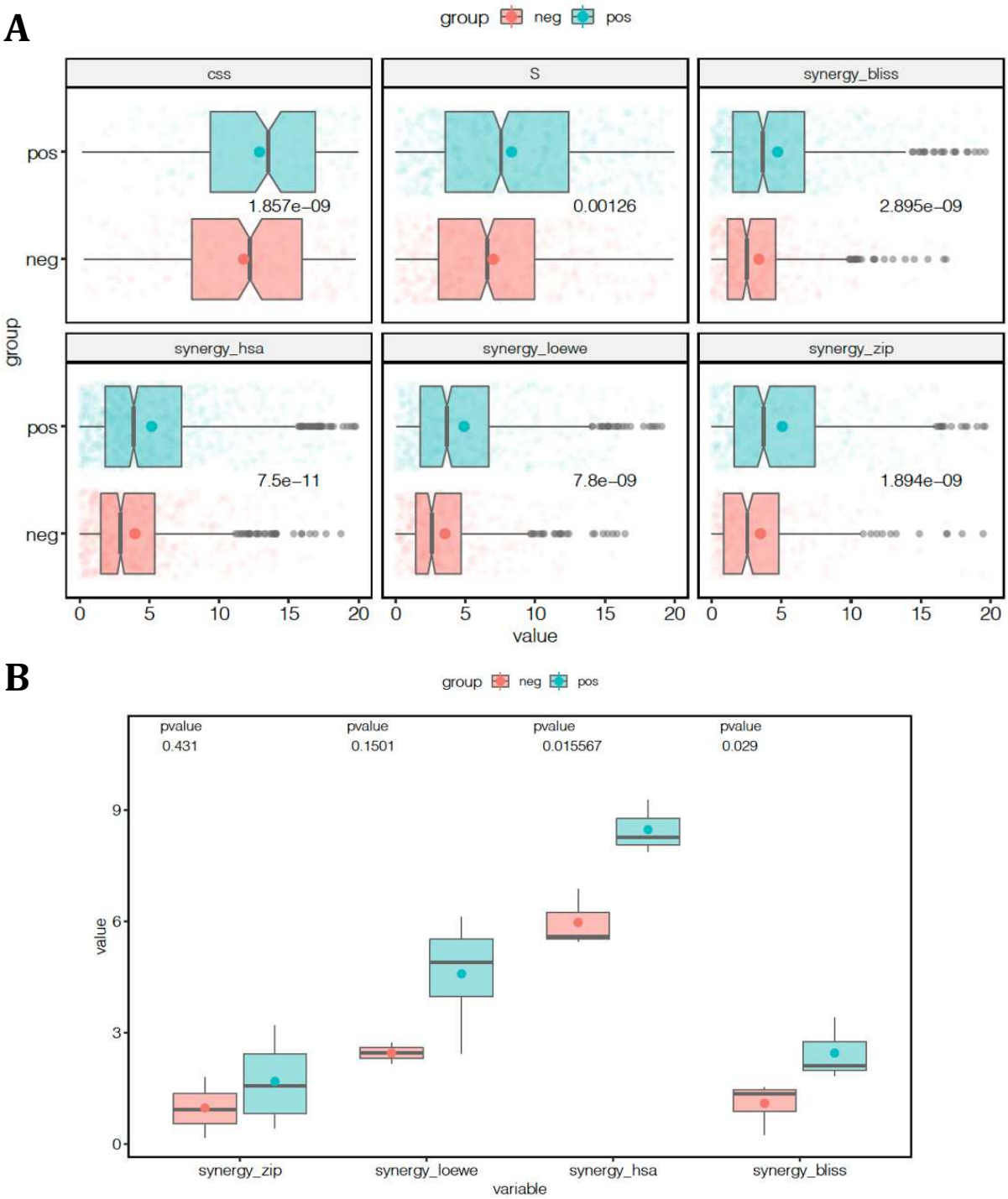

Figure 9: Synergy of drug combinations. (A) The combinational sensitivity (CSS) and synergy scores (S, synergy_bliss, synergy_hsa, synergy_loewe, and synergy_zip) of drug combinations in the ALMANAC dataset. The top five drugs of cluster 1 (Cabazitaxel, 5-FU, Cytarabine hydrochloride, Methotrexate, Bleomycin) and cluster 2 (CHEMBL17639, Gefitinib, Ixabepilone, Dexrazoxane, Eloxatin) for inter-cluster and intra-cluster combinations are shown in blue and red as the positive and negative groups, respectively. Each plot contains a scatter plot, a notch box plot, and mean values for each group. The p-value represents the one-sided Student's t-test significance for each score separately. (B) The measured synergy of drug combination scores in the experimental validation of selected drugs based on network modelling of the Beat AML data in three AML cell lines. Four measures of synergy, that is, ZIP, HSA, Bliss, and Loewe, are seen as notch box plots for the experimental confirmation of the 25 chosen predictions in three cell lines. Inter-cluster drug combinations are shown in blue as the positive group, and the intra-cluster combinations are shown in red as the negative group.

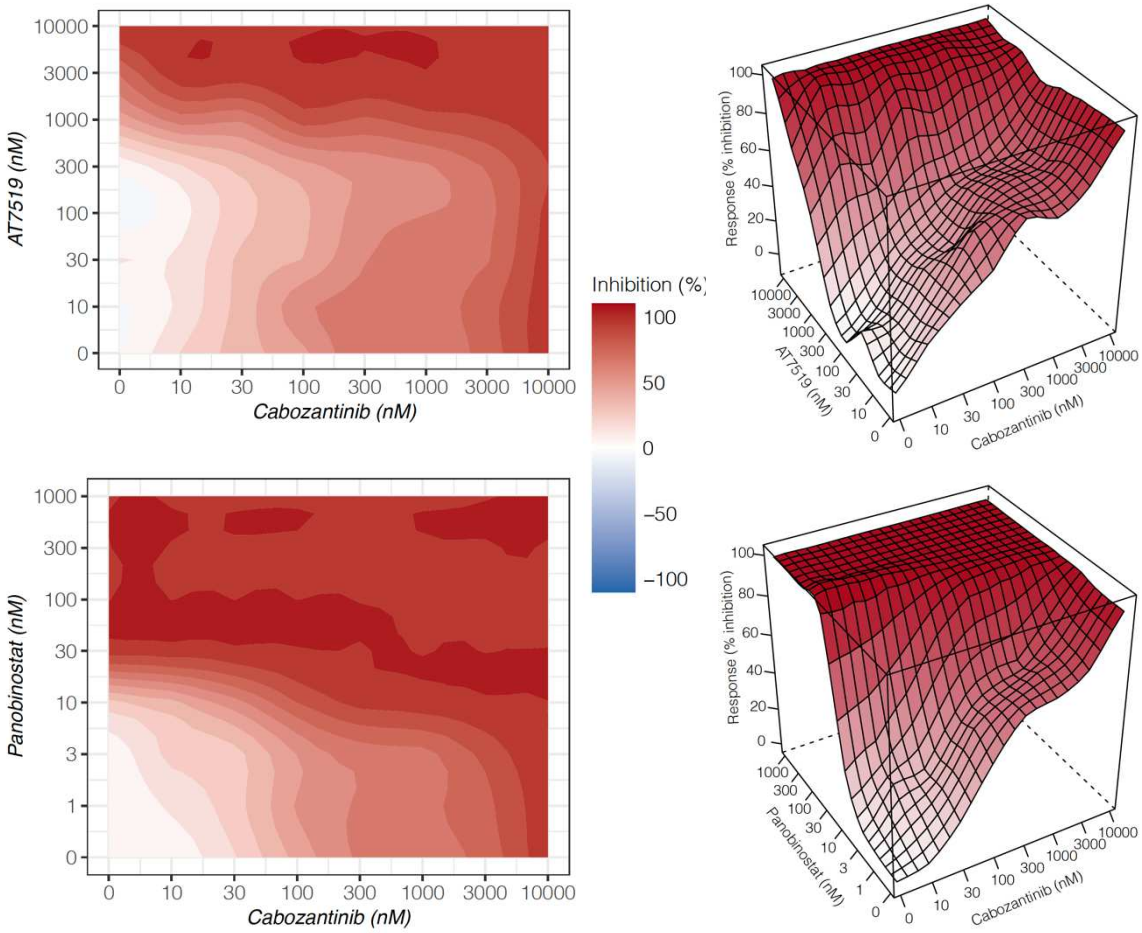

Figure 10: The top synergistic drug combinations identified in the positive group. These matrices represent the highest synergistic combination based on four measures of synergy. HSA and LOEWE methods indicate that the cabozanitinb and AT7519 combination is the highest synergistic combination. The combination of cabozanitinb and panobinostat is the most synergistic based on ZIP and Bliss measures. For each combination, the sensitivity landscapes are shown in both 2D and 3D. The complete sensitivity landscapes for all 135 drug combinations can be found in supplementary Fig. 2.

Discussion

The availability of single-drug response datasets for cancer cell lines has prompted us to develop methods for predicting and selecting the most effective combination therapy. Several AI-based combination prediction approaches have recently been introduced that combine high-throughput molecular profiling data with drug response data to improve prediction and validation. To reflect the relationships between drug combinations, Narayan *et al.* used dose-response data from pharmacogenomic encyclopaedias and represented them as drug atlas (45). Combining with the pathway/gene ontology data, their approach enables the prediction of combinatorial therapy, i.e., vulnerability when attacked by two drugs that can be related to tumour-driving mutations. They repeated the predicted synergies in several tumours, including glioblastoma, breast cancer, melanoma, and leukaemia mouse models, highlighting the cancer-

independent prediction power of drug combination treatment. Ianevski *et al.* also showed that bulk viability single-agent screening assays had unexpectedly large predictability for AML cell subpopulation co-inhibition effects when combined with scRNA-seq transcriptomic data (18). They developed a machine-learning model by combining single-cell RNA sequencing with *ex vivo* single-agent testing for AML with a different genetic background. They displayed an accurate prediction of synergistic patient-specific combinations while avoiding the inhibition of non-malignant cells. However, while our biomarker-independent approach relies only on the phenotypic level of information, that is, drug-response data, our predictions were compatible with the molecular profiling and biochemical annotations when it came to assessing the intra-cluster homogeneity of drugs, patients, and cell lines

Moreover, a training machine-learning model for predicting drug combination response, comboFM, was recently introduced using drug combination screening data as a training dataset (46). comboFM uses a factorisation machine to model cell context-specific drug interactions through higher-order tensors. Julkunen *et al.* demonstrated that comboFM enables leveraging information from previous experiments performed on similar drugs and cells as training data when predicting responses of new combinations, insofar as untested cells (testing data). They displayed high predictive performance and robust applicability of comboFM in various prediction scenarios using experimental validation of a set of previously untested drugs. However, we expounded that the prediction accuracy of the inter-cluster design strategy of drug combinations based on multipartite networks can be achieved independently from the high-quality training dataset.

Strictly speaking, in the present study, we revisited the analysis of nominal variables, namely drug name and sample identity, in drug screening results for data mining using graph theory, which we termed the nominal data mining approach. We first considered data quality control, such as outlier detection, outlier treatment, biological and technical replicates. Because of the discrete explanatory independent variable (i.e. drug doses) (47), we assumed that regression-based measurements might even be discarded; hence, we demonstrated that median values can represent an appropriate weight score in comparing drug functionality for network reconstruction. These values were used to quantify and weight the bipartite network, which reflects the interaction strength of the drugs and biological samples. Then, two similarity networks were provided by weighted network projection to detect the topological structure of the network communities. We showed that network communities represent a rationale starting point for proposing a combinational drug regimen. Our computational and experimental

validation steps amplified the logic of our proposed platform. Hence, while training datasets were not required in this method to predict drug combination, drug response data alone were adequate for the prediction, without integrating prior knowledge of biochemical profiling.

Noting that the occurrence of synergistic toxicities, which can arise from additive toxicities when targets are shared by the combined drugs, is a major barrier to applying combination therapy in the clinic (48). If drug screening data on healthy cells are available, we suggest that a similar strategy for predicting toxicity without losing efficacy is also essential before future translational experiments. Ianevski *et al.* previously illustrated the importance of a desired synergy-efficacy-toxicity balance for predicting patient-customised drug combinations (18). Hence, drug-response data on healthy cells are demanded to complement synergistic interactions of drug combinations with toxicity predictions; where drug synergy and toxicity data are optimally matched for combinatorial therapy, stronger and longer-lasting outcomes of drug combinations can be predicted.

Furthermore, prospective work will necessitate the provision of further patient-derived experimental validations. Despite the fact that our prediction depends solely on the drug sensitivity dataset, our suggested combinations address the common mutational assigned aetiology of AML. Remarkably, this combination was proposed purely on the grounds of the phenotypic response of cancer cells or patient samples to the drugs, with no previous knowledge of the disease's genetic origin.

References

1. Nussinov R, Jang H, Tsai CJ, Cheng F. Review: Precision medicine and driver mutations: Computational methods, functional assays and conformational principles for interpreting cancer drivers. Plos Computationa Biology. 2019;15:1-54.
2. Yaffe MB. Why geneticists stole cancer research even though cancer is primarily a signaling disease. Science Signaling. 2019;12(565).
3. Hanahan D, Weinberg RA. Hallmarks of cancer: the next generation. cell. 2011;144(5):646-74.
4. Kibble M, Saarinen N, Tang J, Wennerberg K, Mäkelä S, Aittokallio T. Network pharmacology applications to map the unexplored target space and therapeutic potential of natural products. Nat Prod Rep. 2015;6:1249-66.
5. Tang J, Aittokallio T. Network pharmacology strategies toward multi-target anticancer therapies: from computational models to experimental design principles. Current pharmaceutical design. 2014;20(1):23-36.
6. Wang Z, Monteiro CD, Jagodnik KM, Fernandez NF, Gundersen GW, Rouillard AD, et al. Extraction and analysis of signatures from the Gene Expression Omnibus by the crowd. Nature communications. 2016;7:12846-.
7. Barneh F, Mirzaie M, Nickchi P, Tan TZ, Thiery JP, Piran M, et al. Integrated use of bioinformatic resources reveals that co-targeting of histone deacetylases, IKBK and SRC inhibits epithelial-mesenchymal transition in cancer. Briefings in Bioinformatics. 2019;20(2):717-31.
8. Barneh F, Salimi M, Goshadrou F, Ashtiani M, Mirzaie M, Zali H, et al. Valproic acid inhibits the protective effects of stromal cells against chemotherapy in breast cancer: Insights from proteomics and systems biology. Journal of cellular biochemistry. 2018;119(11):9270-83.
9. Pemovska T, Kontro M, Yadav B, Edgren H, Eldfors S, Szwajda A, et al. Individualized Systems Medicine Strategy to Tailor Treatments for Patients with Chemorefractory Acute Myeloid Leukemia. Cancer Discovery. 2013;3(12):1416-29.
10. Pauli C, Hopkins BD, Prandi D, Shaw R, Fedrizzi T, Sboner A, et al. Personalized in vitro and in vivo cancer models to guide precision medicine. Cancer Discovery. 2017;7(5):462-77.
11. Xu T, Pi Z, Liu S, Song F, Liu Z. Chemical Profiling Combined with "Omics" Technologies (CP-Omics): a Strategy to Understand the Compatibility Mechanisms and Simplify Herb Formulas in Traditional Chinese Medicines. Phytochemical analysis : PCA. 2017;28(5):381-91.
12. Shinkafi T.S. AS. Holistic Approach to Traditional and Herbal Medicines: The Role of Omics, Systems Biology, and Computational Technologies. In: Hakeem K. MA, Vardar-Sukan F., Ozturk M., editor. Plant Bioinformatics: Springer, Cham; 2017.
13. Flobak Å, Niederdorfer B, Nakstad VT, Thommesen L, Klinkenberg G, Lægreid A. A high-throughput drug combination screen of targeted small molecule inhibitors in cancer cell lines. Scientific Data. 2019;6(1):237.
14. Budman DR, Calabro A, Kreis W. Synergistic and antagonistic combinations of drugs in human prostate cancer cell lines in vitro. Anticancer Drugs. 2002;13(10):1011-6.
15. Budman DR, Calabro A, Rosen L, Lesser M. Identification of unique synergistic drug combinations associated with downexpression of survivin in a preclinical breast cancer model system. Anticancer Drugs. 2012;23(3):272-9.
16. Jaiswal A, Gautam P, Pietilä EA, Timonen S, Nordström N, Akimov Y, et al. Multi‐modal meta‐analysis of cancer cell line omics profiles identifies ECHDC1 as a novel breast tumor suppressor. Molecular systems biology. 2021;17(3):e9526.
17. He L, Tang J, Andersson EI, Timonen S, Koschmieder S, Wennerberg K, et al. Patient-Customized Drug Combination Prediction and Testing for T-cell Prolymphocytic Leukemia Patients. Cancer research. 2018;78(9):2407-18.

18. Ianevski A, Lahtela J, Javarappa KK, Sergeev P, Ghimire BR, Gautam P, et al. Patient-tailored design for selective co-inhibition of leukemic cell subpopulations. Science Advances. 2021;7(8):eabe4038.
19. Tyner JW, Tognon CE, Bottomly D, Wilmot B, Kurtz SE, Savage SL, et al. Functional genomic landscape of acute myeloid leukaemia. Nature. 2018;562(7728):526-31.
20. Iorio F, Knijnenburg TA, Vis DJ, Bignell GR, Menden MP, Schubert M, et al. A Landscape of Pharmacogenomic Interactions in Cancer. Cell. 2016;166(3):740-54.
21. Holbeck SL, Camalier R, Crowell JA, Govindharajulu JP, Hollingshead M, Anderson LW, et al. The National Cancer Institute ALMANAC: a comprehensive screening resource for the detection of anticancer drug pairs with enhanced therapeutic activity. Cancer research. 2017;77(13):3564-76.
22. Zheng S, Aldahdooh J, Shadbahr T, Wang Y, Aldahdooh D, Bao J, et al. DrugComb update: a more comprehensive drug sensitivity data repository and analysis portal. bioRxiv. 2021:2021.03.25.436916.
23. Geeleher P, Gamazon ER, Seoighe C, Cox NJ, Huang RS. Consistency in large pharmacogenomic studies. Nature. 2016;540(7631):E1-E2.
24. Mpindi JP, Yadav B, Östling P, Gautam P, Malani D, Murumägi A, et al. Consistency in drug response profiling. Nature. 2016;540(7631):E5-E6.
25. Reshef DN, Reshef YA, Finucane HK, Grossman SR, McVean G, Turnbaugh PJ, et al. Detecting novel associations in large data sets. Science (New York, NY). 2011;334(6062):1518-24.
26. Rosvall M, Bergstrom CT. Maps of random walks on complex networks reveal community structure. Proceedings of the National Academy of Sciences. 2008;105(4):1118.
27. Clauset A, Newman ME, Moore C. Finding community structure in very large networks. Physical review E. 2004;70(6):066111.
28. Newman ME, Girvan M. Finding and evaluating community structure in networks. Physical review E. 2004;69(2):026113.
29. Gaulton A, Hersey A, Nowotka M, Bento AP, Chambers J, Mendez D, et al. The ChEMBL database in 2017. Nucleic acids research. 2017;45(D1):D945-D54.
30. Tang J, Tanoli ZuR, Ravikumar B, Alam Z, Rebane A, Vähä-Koskela M, et al. Drug Target Commons: A Community Effort to Build a Consensus Knowledge Base for Drug-Target Interactions. Cell Chemical Biology. 2018;25(2):224-9.e2.
31. Kanehisa M, Sato Y, Furumichi M, Morishima K, Tanabe M. New approach for understanding genome variations in KEGG. Nucleic acids research. 2019;47(D1):D590-D5.
32. Türei D, Korcsmáros T, Saez-Rodriguez J. OmniPath: guidelines and gateway for literature-curated signaling pathway resources. Nature methods. 2016;13(12):966-7.
33. Bajusz D, Rácz A, Héberger K. Why is Tanimoto index an appropriate choice for fingerprint-based similarity calculations? Journal of Cheminformatics. 2015;7(1):1-13.
34. Zagidullin B, Aldahdooh J, Zheng S, Wang W, Wang Y, Saad J, et al. DrugComb: an integrative cancer drug combination data portal. Nucleic acids research. 2019.
35. Yadav B, Wennerberg K, Aittokallio T, Tang J. Searching for Drug Synergy in Complex Dose-Response Landscapes Using an Interaction Potency Model. Comput Struct Biotechnol J. 2015;13:504-13.
36. Berenbaum MC. What is synergy? Pharmacol Rev. 1989;41(2):93-141.
37. Loewe S. The problem of synergism and antagonism of combined drugs. Arzneimittelforschung. 1953;3(6):285-90.
38. BLISS CI. THE TOXICITY OF POISONS APPLIED JOINTLY1. Annals of Applied Biology. 1939;26(3):585-615.

39. Malyutina A, Majumder MM, Wang W, Pessia A, Heckman CA, Tang J. Drug combination sensitivity scoring facilitates the discovery of synergistic and efficacious drug combinations in cancer. PLoS Comput Biol. 2019;15(5):e1006752.
40. Tabei Y, Pauwels E, Stoven V, Takemoto K, Yamanishi Y. Identification of chemogenomic features from drug–target interaction networks using interpretable classifiers. Bioinformatics. 2012;28(18):i487-i94.
41. Öztürk H, Ozkirimli E, Özgür A. A comparative study of SMILES-based compound similarity functions for drug-target interaction prediction. BMC bioinformatics. 2016;17(1):128.
42. Montaruli M, Alberga D, Ciriaco F, Trisciuzzi D, Tondo AR, Mangiatordi GF, et al. Accelerating Drug Discovery by Early Protein Drug Target Prediction Based on a Multi-Fingerprint Similarity Search †. Molecules. 2019;24(12).
43. Trosset J-Y, Cavé C. In Silico Drug–Target Profiling. In: Moll J, Carotta S, editors. Target Identification and Validation in Drug Discovery: Methods and Protocols. New York, NY: Springer New York; 2019. p. 89-103.
44. Parikh JR, Klinger B, Xia Y, Marto JA, Blüthgen N. Discovering causal signaling pathways through gene-expression patterns. Nucleic Acids Res. 2010;38(Web Server issue):W109-17.
45. Narayan RS, Molenaar P, Teng J, Cornelissen FMG, Roelofs I, Menezes R, et al. A cancer drug atlas enables synergistic targeting of independent drug vulnerabilities. Nature Communications. 2020;11(1):2935.
46. Julkunen H, Cichonska A, Gautam P, Szedmak S, Douat J, Pahikkala T, et al. Leveraging multi-way interactions for systematic prediction of pre-clinical drug combination effects. Nature Communications. 2020;11(1):6136.
47. Montgomery DC, Peck EA, Vining GG. Introduction to Linear Regression Analysis. Edition t, editor: Wiley; 2012.
48. Larkin J, Chiarion-Sileni V, Gonzalez R, Grob JJ, Cowey CL, Lao CD, et al. Combined nivolumab and ipilimumab or monotherapy in untreated melanoma. New England journal of medicine. 2015;373(1):23-34.

Supplementary figures

Supplementary figure 1: Drug and patient nodes in the projected networks of the Beat AML dataset. The nodes are ordered based on the strength of each node, which is the sum of the edge weights of the adjacent edges for each node.

Supplementary figure 2: The complete interaction landscapes for all the 135 drug combinations.

Supplementary Files

This is a list of supplementary files associated with this preprint. Click to download.

- SupplementaryFig1.pdf
- SupplementaryFig2.pdf